Cancer Immunology, Immunotherapy
https://doi.org/10.1007/s00262-020-02818-y

ORIGINAL ARTICLE

Immuno-PET imaging of ^{68}Ga-labeled nanobody Nb109 for dynamic monitoring the PD-L1 expression in cancers

Qingzhu Liu[1] · Lei Jiang[2] · Ke Li[1] · Hang Li[1] · Gaochao Lv[1] · Jianguo Lin[1,3] · Ling Qiu[1,3]

Received: 6 September 2020 / Accepted: 2 December 2020

Abstract

The checkpoint blockade immunotherapy has become a potent treatment strategy for cancers, and programmed death ligand-1 (PD-L1) is a prominent checkpoint ligand that is highly expressed in some cancers. The identification of immune checkpoint marker PD-L1 is critical for improving the success of immunotherapy. Accordingly, the binding specificity and dynamic monitoring property of a non-blocking nanobody tracer ^{68}Ga-NOTA-Nb109 to PD-L1 were assessed in this study. The endogenous expression level of PD-L1 in several cancer cells was measured by flow cytometry, Western blot, and cellular uptake assay. Sensitivity and specificity of ^{68}Ga-NOTA-Nb109 in monitoring the expression of PD-L1 in vivo were evaluated by PET imaging of different tumor-bearing models (U87, high PD-L1 expression; HCT 116, medium PD-L1 expression; and NCI-H1299, low PD-L1 expression). In vivo PET imaging results agreed well with those detected in vitro. In addition, PET imaging of PD-L1 expression in U87 and NCI-H1299 xenografts using ^{18}F-FDG was also performed for comparison. The maximum tumor-to-muscle uptake ratio of ^{68}Ga-NOTA-Nb109 was more than twofold that of ^{18}F-FDG in U87 xenograft. The change of PD-L1 expression in NCI-H1299 cells and xenografts induced by cisplatin (CDDP) was sensitively monitored by ^{68}Ga-NOTA-Nb109. This study demonstrated the feasibility of tracer ^{68}Ga-NOTA-Nb109 for specifically targeting endogenous PD-L1 and dynamic monitoring the change of PD-L1 expression, and could guide the immunotherapy and immunochemotherapy for refractory cancers.

Keywords PD-L1 · PET imaging · Nanobody tracer · ^{68}Ga · ^{18}F-FDG

Abbreviations

CDDP	Cisplatin
IHC	Immunohistochemistry
mAbs	Monoclonal antibodies
NSCLC	Non-small cell lung cancer
PD-1	Programmed death protein 1
PD-L1	Programmed death ligand-1
ROI	Region of interest

Introduction

Immunotherapy has become a mainstay of clinical medicine following traditional therapies. For a healthy immune system, immunoactivation and immunosuppression are in a delicate balance, in which the immune checkpoints of programmed death protein 1 (PD-1) and PD-1 ligand (PD-L1) act as a brake for activated T cells to reduce the immune killing. Tumor cells exploit the "braking" function by overexpressing PD-L1 to escape anti-tumor immune surveillance [1, 2]. Clinical evidences have shown that PD-L1 is highly expressed in many tumors [3–5], and poor prognosis and increased mortality of cancers are related to the expression of PD-L1 [6, 7]. The blocking of PD-1/PD-L1 signaling pathway in cancers can reactivate the immune killing function of activated T cells and enhance the immune response against solid tumors [8]. For patients with advanced

Qingzhu Liu and Lei Jiang contributed equally to this work.

✉ Jianguo Lin
linjianguo@jsinm.org

✉ Ling Qiu
qiuling@jsinm.org

[1] NHC Key Laboratory of Nuclear Medicine, Jiangsu Key Laboratory of Molecular Nuclear Medicine, Jiangsu Institute of Nuclear Medicine, Wuxi 214063, China

[2] Department of Nuclear Medicine, Shanghai Pulmonary Hospital, Tongji University School of Medicine, Shanghai 200433, China

[3] Department of Radiopharmaceuticals, School of Pharmacy, Nanjing Medical University, Nanjing 211166, China

Published online: 02 January 2021

non-small cell lung cancer (NSCLC), only a 20–40% overall response rate to the immunotherapy with PD-1/PD-L1 inhibitors could be achieved [9], but it can reach 90% for PD-1/PD-L1 positive patients [10–12]. This indicated that the expression level of PD-1/PD-L1 may be a critical factor for targeted therapy of tumor immune checkpoints. Therefore, prior to carrying out immunotherapy, determining the expression level of PD-1/PD-L1 might be conducive to the specific treatment of patients [13].

Immunohistochemistry (IHC) staining of tumor biopsies is a conventional method to evaluate the PD-1/PD-L1 expression level, but it cannot fully and accurately evaluate the true expression of PD-1/PD-L1 due to the high heterogeneity and dynamic change in primary and metastatic tumors [14–16]. In addition, pathologists might still be confused by the inconsistencies in antibodies and evaluation criteria used for IHC [17]. Many studies have shown that molecular imaging technology as a non-invasive tool is complementary to IHC and can intuitively monitor the expression of relevant immune checkpoints [18–20]. The detection and quantification of PD-1/PD-L1 expression level in patients by molecular imaging can provide more accurate, real-time, and comprehensive information, which will be used to screen patients that are suitable for immunotherapy and to estimate the effect of immunotherapy.

Recently, many PD-1/PD-L1-targeted immuno-PET tracers with therapeutic monoclonal antibody (mAb)-based have been reported [10]. Atezolizumab, the first FDA-approved PD-L1 mAbs for bladder and non-small cell lung cancers [21, 22], has been modified by pharmacists for immuno-PET imaging of PD-L1 and showed a specific targeting in vivo [18, 19, 23]. However, the inherent characteristics of mAbs limit their clinical applications as imaging tracers. One major disadvantage of antibody-based imaging agents is their slow-clearance rate. Due to their poor tumor penetration and long-metabolism time in vivo, we should wait for several days to obtain high-resolution images. Another disadvantage for antibody-based imaging agents is that therapeutic antibodies that targeted the same binding site would affect the tumor imaging and interfere the prognostic evaluation. Therefore, non-mAb-based tracers with better biological properties have been explored, such as peptide-based tracers ^{68}Ga- and ^{64}Cu-labeled WL12 [24, 25], ^{18}F- and ^{64}Cu-labeled TPP-1 [26]. Recently, our group has developed a non-blocking nanobody-based tracer ^{68}Ga-NOTA-Nb109 which possessed a different binding epitope from the PD-L1 antibody KN035, and the experimental results clearly showed PD-L1 expression-dependent accumulation of ^{68}Ga-NOTA-Nb109 in tumors [20].

Although the immune checkpoint treatment has shown promising efficacy to cancers, the adverse events of resistance and relapse often require the combination of immunotherapy with other treatment options such as radiotherapy and chemotherapy [27]. Radiotherapy can reduce the volume of tumor by exposing to radiation in a small area, but the side effects are still obvious, especially the damage to the immune system. Cancer is a local manifestation of a systemic disease, and the biggest threat to patients is the spread and metastasis of tumor cells. Compared with radiotherapy, chemotherapy is a holistic treatment for cancers and has some systemic cytotoxicity. Previous researches have shown that chemotherapy drugs can induce more PD-L1 epitopes, whereas not all tumors exhibited the enhancement of PD-L1 expression by radiotherapy [28]. In this study, we investigated the specific affinity of ^{68}Ga-NOTA-Nb109 to wild-type cancer cells that expressed endogenous PD-L1 by PET imaging. In the meantime, the change of PD-L1 expression in tumors induced by chemotherapy was evaluated using ^{68}Ga-NOTA-Nb109. The research indicated that tracer ^{68}Ga-NOTA-Nb109 can specifically target PD-L1 and can dynamically monitor the change of PD-L1 expression caused by external conditions. This study will provide a guide to the combination therapy of chemotherapy and immunotherapy.

Materials and methods

Synthesis of probe ^{68}Ga-NOTA-Nb109

Synthesis and purification of probe ^{68}Ga-NOTA-Nb109 were carried out as reported previously [20]. Briefly, the radioactive ^{68}Ga ion was eluted from the ^{68}Ge/^{68}Ga generator (Germany, ITG GmbH) by hydrochloric acid solutions (0.05 mM), and about 300 MBq (8 mCi) of ^{68}Ga ion was eluted in 2 mL. The pH of radionuclide ^{68}Ga solution (1.4 mL) was adjusted to 4 with sodium acetate buffer (0.25 M, 380 µL). 60–80 µg pure NOTA-Nb109 (kindly provided by Suzhou Smart Nuclide Biopharmaceutical Co., Ltd, China) was added to start the radio-labeling at 37 °C for 15 min. The radiolabeled product was purified using PD-10 desalting columns (GE Healthcare life sciences), and the purity of ^{68}Ga-NOTA-Nb109 was evaluated using radio-HPLC with SuperGalaxy-SEC-S2000 (3 µm, 300 × 7.8 mm) chromatographic column (Guangzhou FLM Scientific Instrument Co., Ltd, China).

Cell culture and animal models

Cancer cell lines including human glioma cancer U87, human colorectal cancer HCT 116, and human lung cancers NCI-H1299, A549, NCI-H460, NCI-H446, NCI-H661, and NCI-H522 were obtained from cell bank of Chinese Academy of Science. Cells were cultured with DMEM (Biological Industries, Israel) or 1640 medium (Biological Industries, Israel) supplemented with 10% fetal bovine serum

(Biological Industries, Israel) and 1% penicillin–streptomycin (Beyotime Biotechnology, China). All cells were incubated at 37 °C in a humidified 5% CO_2 incubator. The cells at the logarithmic growth phase were employed for in vitro biological evaluation.

For in vivo biological studies, female BALB/c nude mice (nu/nu, five-to-seven weeks of age) were purchased from Changzhou Cavens Laboratory Animal Co., Ltd. (Changzhou, China). Mice were inoculated subcutaneously with 5×10^6 cancer cells in 200 μL of saline. When the tumor reached an average volume of 300–500 mm^3 ($n = 3$–4 per group), in vivo experiments can be performed. Six to eight mice bearing NCI-H1299 tumors were randomly divided into two groups, and one group was administrated intravenously with cisplatin (CDDP) in saline via the tail vein. 2 mg/kg CDDP was given once every other day, for a total of 3–5 times, and then NCI-H1299-bearing mice with CDDP-induced high PD-L1 expression level (NCI-H1299-CDDP) were obtained. In the meantime, another group of NCI-H1299-bearing mice was administrated with saline under the same conditions for comparison.

PD-L1 expression analysis by Western blot

Cancer cells of U87, HCT 116, and NCI-H1299 at the logarithmic growth phase, as well as NCI-H1299 incubated with CDDP at the concentration of 10, 20, 40, and 80 μM for 48 h were lysed on ice for 30 min with RIPA (Beyotime, Shanghai, China). The cell lysates were centrifuged, and the protein concentration was detected by BCA method (Thermo Scientific, USA). Approximately 50 μg of cell lysates were electrophoresed on 15% SDS-PAGE and transferred to PVDF membranes. The membranes were incubated with antibodies of Rabbit anti-human PD-L1 [EPR19759] (1:500, Abcam, China, Cat. #ab213524), GAPDH (1:1000, Beyotime Biotechnology, China, Cat. #AF1186), and β-Actin (1:1000, Beyotime Biotechnology, China, Cat. AF5001) at 4 °C overnight. After the membrane was incubated with the corresponding secondary antibody (1:1000, Mouse anti-rabbit IgG-HRP antibody and Mouse IgG κ BP-HRP antibody, Santa Cruz Biotechnology, USA, Cat. #sc-2357 and sc-516102, respectively), Western blot ECL reagent solution (Shanghai share-bio Technology Co., Ltd, China) was utilized to detect the signal and the gray scale of signals was quantified using ImageJ software.

PD-L1 expression detection by flow cytometry

The PD-L1 expression in cancer cells was tested using flow cytometry analysis with PE-labeled mouse anti-human PD-L1 (CD274) antibody (BD Biosciences, USA, Cat. #557924). Briefly, cancer cells of U87, HCT 116, and NCI-H1299 were digested with EDTA-free trypsin, and about 1×10^6 cells (100 μL) were incubated with 20 μL antibody for 30 min at 4 °C in the dark. The fluorescence absorption of cancer cells was analyzed using FACSCalibur flow cytometer (BD Biosciences, USA) immediately. In the meantime, the cells incubated with mouse IgG1 and PBS served as the isotype control and background signal, respectively. The quantitative analysis of mean fluorescence intensity was performed with FlowJo.

In vitro cell binding

NCI-H1299 cells (3×10^5 cells per well in 3 mL full 1640 medium) were seeded into 6 cell plates and incubated at 37 °C in 5% CO_2 incubator overnight. Followed by removal of the medium, cells were incubated with 0 and 20 μM CDDP for another 48 h. Meantime, cancer cells U87, HCT 116, and NCI-H1299 (1×10^6 cells, 200 μL) were incubated with serum-free 1640 or DMEM containing 37 KBq ^{68}Ga-NOTA-Nb109 for 0.5, 1, 2, and 4 h, respectively. Then, cells were washed with ice PBS, harvested, centrifuged, and the radioactivity remained in cells was measured with a γ counter. Then, cells were lysed and the protein concentration was determined by BCA method. Free ^{68}Ga-NOTA-Nb109 (37 KBq) was used as a control to identify the decay correction. The cellular uptake of ^{68}Ga-NOTA-Nb109 was determined by calculating the radioactivity per milligram of protein.

Cytotoxic effect of CDDP

The cytotoxic activity of CDDP against different types of lung cancer cell lines was detected by MTT assay. Cancer cells were plated in 96-well plates (8×10^3 cells per well) and cultured overnight. The cells were incubated with new medium containing different concentrations of CDDP (0, 3.125, 6.25, 12.5, 25, 50, and 100 μM) for 48 h. Then, 20 μL MTT (5 mg/mL) was added and incubated for another 4 h. The formazan generated in living cells was dissolved by DMSO, and the optical density (OD) of each well was measured at 490 nm by the microplate reader. The inhibitory activity of CDDP against lung cancers was predicted by calculating the half-inhibitory concentration IC_{50}.

Micro-PET imaging

Whole-body PET images were acquired on a micro-PET scanner (Siemens Medical Solutions, Germany). Mice bearing subcutaneous tumors were anesthetized with isoflurane, and 4.0–5.5 MBq tracers were injected into models via the tail vein, in which ^{68}Ga-NOTA-Nb109 was performed on U87, HCT 116, NCI-H1299, and NCI-H1299-CDDP xenografts, while ^{18}F-FDG was performed on U87 and NCI-H1299 xenografts. In the blocking

group, the mice bearing subcutaneous U87 tumors were pretreated with 200-fold molar excess of NOTA-Nb109 for 30 min via the tail vein. 1-h dynamic emission images were acquired for all models, and 12 frame images were collected with an interval of 5 min. The uptake of tracers in tumor or muscle was estimated by sketching the region of interest (ROI) on images using ASIPro VM™ software (Siemens Medical Solutions, USA), and the quantification of ROI was calculated as percent of injection dose per gram of tissue (%ID/g).

Autoradiography analysis

The quantitative biodistribution of tracer ^{68}Ga-NOTA-Nb109 in tumors of NCI-H1299 and NCI-H1299-CDDP xenografts was investigated using the autoradiography analysis. Briefly, the models were euthanized by overdose of the anesthetic following 1-h in vivo dynamic PET imaging. The tumor tissues were harvested and frozen at − 80 °C for 10–15 min, and then 20-μm frozen sections were exposed to a phosphor imaging system (Cyclone PLUS, PerkinElmer, USA) for 2 h. And the plates were read by a phosphor imaging plate reader. Three sections of different dimensions were extracted from each tissue sample, and the signals were quantified using ImageJ software.

Statistical analysis

Statistical analysis was performed with GraphPad Prism 5 software. The differences in data were determined by *t* test method, and $P < 0.05$ was considered to be statistically significant. Results were presented as mean ± standard error (SD).

Results

PD-L1 expression analysis in vitro

Although the specificity of tracer ^{68}Ga-NOTA-Nb109 to PD-L1 has been demonstrated on A375-hPD-L1 cells [20], there is no sufficient evidence to prove the specificity of ^{68}Ga-NOTA-Nb109 to endogenous PD-L1 in wild-type cancer cells. Therefore, to identify the specific binding of tracer ^{68}Ga-NOTA-Nb109 to PD-L1 in wild-type cancer cells, the expression level of PD-L1 in various cancer cells was evaluated first using flow cytometry and Western blot methods (Fig. 1). As can be seen from Fig. 1a, the fluorescence absorption of cancer cell U87

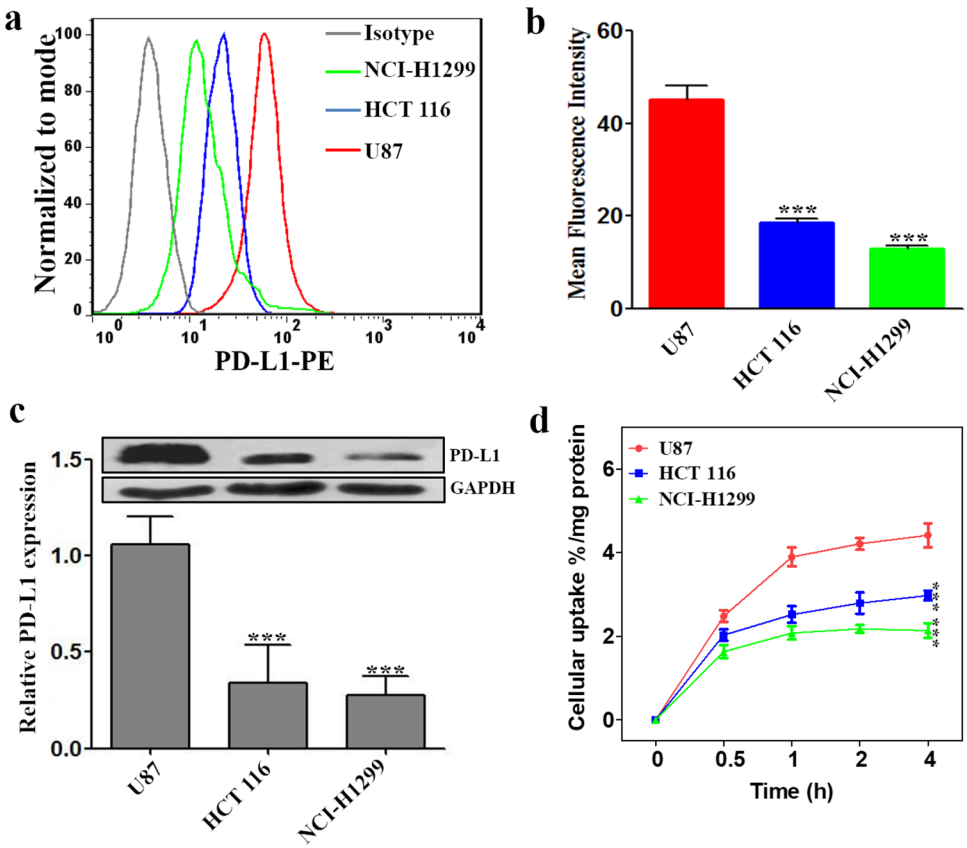

Fig. 1 Analysis of PD-L1 expression in different cancer cell lines. **a** Flow cytometry analysis of PD-L1 expression in different cancer cells (U87, HCT 116, and NCI-H1299). **b** Quantitative analysis of mean fluorescence intensity using FlowJ. **c** Western blot analysis of PD-L1 (50 kDa) expression in cancer cells with GAPDH (36 kDa) as the internal control. **d** Cellular uptake of ^{68}Ga-NOTA-Nb109 in cancer cells of U87, HCT 116, and NCI-H1299. All results were expressed as mean ± SD from three independent experiments. ***$P < 0.001$

was significantly stronger than others, whereas cancer cell NCI-H1299 showed the weakest fluorescence absorption. The quantification of mean fluorescence intensity demonstrated that the expression of PD-L1 decreased in the order of U87 > HCT 116 > NCI-H1299 (Fig. 1b), and the expression level of PD-L1 in U87 was about 2.4- and 3.5-fold of that HCT 116 and NCI-H1299, respectively. The PD-L1 expression level in three different cancer cells (U87, HCT 116 and NCI-H1299) was also tested by Western blot (Fig. 1c), and the results were accordant with the flow cytometry analysis. Therefore, these cancer cell lines were selected to evaluate the sensitivity and specificity of tracer ^{68}Ga-NOTA-Nb109 in monitoring the expression of PD-L1.

To evaluate the binding specificity of ^{68}Ga-NOTA-Nb109 to PD-L1, in vitro cellular uptake assay was initially performed in different cancer cells with various endogenous PD-L1 expression level. As shown in Fig. 1d, U87 cells with higher endogenous PD-L1 expression showed significantly higher uptake of ^{68}Ga-NOTA-Nb109 than HCT 116 and NCI-H1299 cells with lower endogenous PD-L1 expression. The cellular uptake of ^{68}Ga-NOTA-Nb109 in U87, HCT 116, and NCI-H1299 cells reached an equilibrium after 1 h, which was determined to be 4.21 ± 0.22, 2.79 ± 0.25, and 2.17 ± 0.09% radioactivity/mg protein, respectively. This indicated that ^{68}Ga-NOTA-Nb109 can sensitively and specifically detect the change of PD-L1 expression in different cancer cells.

CDDP effect on PD-L1 expression

Many studies have reported the role of immunotherapy for lung cancers, and immune checkpoint-based therapy has been widely studied, especially for PD-L1 target [29, 30]. However, Western blot and flow cytometry analysis both indicated that lung cancer cells NCI-H1299 exhibited the lowest PD-L1 expression level among the test cancer cell lines (Fig. 1). Considering the epitopes of PD-L1 could be induced by chemotherapy drugs [31], we evaluated the expression of PD-L1 in NCI-H1299 induced by CDDP by Western blot. As described in Fig. 2a, the expression level of PD-L1 in NCI-H1299 was regulated by different concentrations of CDDP. With the increase of CDDP concentration from 0 to 20 μM, the expression level of PD-L1 in NCI-H1299 was upregulated and that induced by 20 μM CDDP was threefold of that untreated. As the concentration of CDDP over 20 μM, the PD-L1 expression decreased slightly but still remained at a higher level. This might be due to the cytotoxic effect of CDDP at a higher concentration on the cancer cells.

To further evaluate the ability of the tracer ^{68}Ga-NOTA-Nb109 in monitoring the change of PD-L1 expression, in vitro cellular uptake of ^{68}Ga-NOTA-Nb109 in NCI-H1299

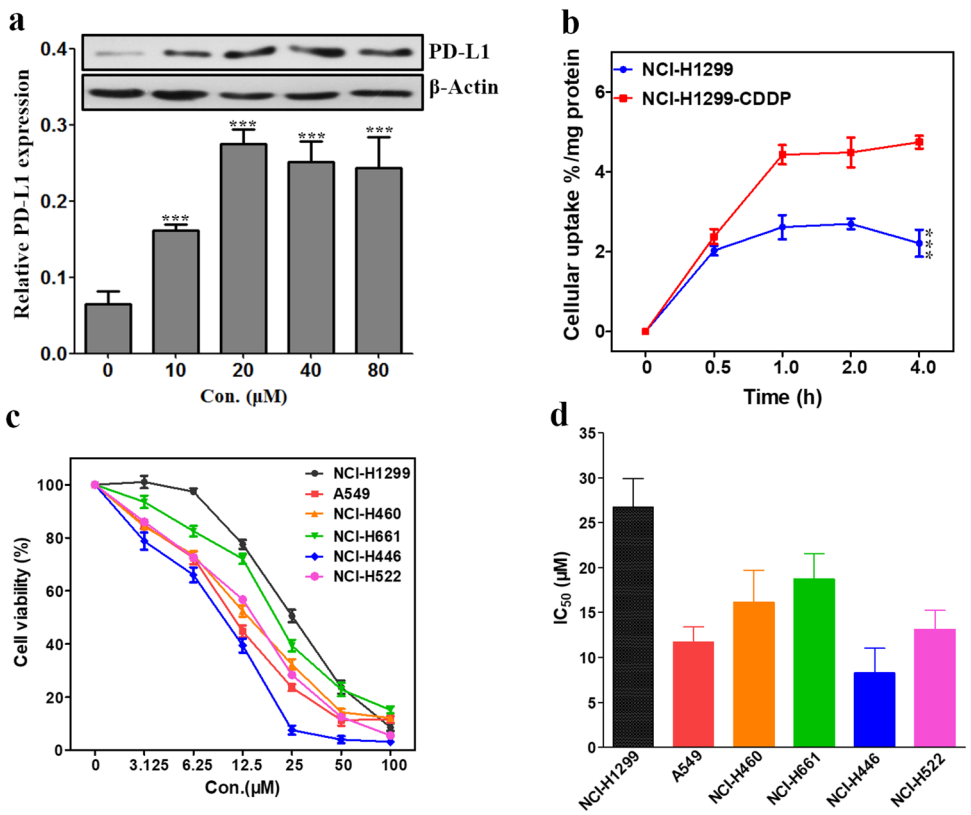

Fig. 2 Effect of CDDP on lung cancer cells. **a** Western blot analysis of PD-L1 (50 kDa) expression in NCI-H1299 cells induced by CDDP at different concentrations for 48 h. **b** Cellular uptake of ^{68}Ga-NOTA-Nb109 in NCI-H1299 and CDDP-treated NCI-H1299 cells. **c** Viability of different lung cancer cells after treatment with various concentrations of CDDP for 48 h. **d** IC_{50} values of CDDP against different lung cancer cells obtained using GraphPad Prism 5.0. All data were expressed as mean ± SD ($n = 3$). ***$P < 0.001$

and NCI-H1299 treated with CDDP (NCI-H1299-CDDP) was investigated. As can be seen from Fig. 2b, NCI-H1299 and NCI-H1299-CDDP have reached an equilibrium uptake of ^{68}Ga-NOTA-Nb109 at 1 h, and the maximum uptake was 2.61 ± 0.30 and 4.43 ± 0.24% radioactivity/mg protein, respectively. The results demonstrated that CDDP can induce the upregulation of PD-L1 expression in NCI-H1299 cells and the upregulation can be detected by tracer ^{68}Ga-NOTA-Nb109.

Chemotherapy drugs especially platinum-based drugs are known as the first line treatment for lung cancers. However, the resistance to chemotherapy remains the major impediment for most lung cancers, although the initial response rate to platinum-based chemotherapy was about 50% [32]. As reported by several researches, the resistance of lung cancers to chemotherapy might be related to the expression of PD-L1 [33]. Thus, the response of different lung cancers including NCI-H1299, A549, NCI-H460, NCI-H446, NCI-H661, and NCI-H522 to CDDP was investigated by MTT assay. As can be seen from Fig. 2c, the viability of all cancer cell lines was significantly affected by CDDP, and the IC_{50} values were in the range of 8.28 ± 2.74 ~ 26.70 ± 3.22 μM (Fig. 2d), indicating that CDDP has a potential inhibitory activity against lung cancers. However, the response of different lung cancers to the treatment of CDDP was different. A549 and NCI-H446 showed higher response to CDDP with the IC_{50} value of 11.67 ± 1.72 and 8.28 ± 2.74 μM, respectively, whereas the CDDP-induced growth inhibition of NCI-H1299 was weak with the IC_{50} value of 26.70 ± 3.22 μM. This indicated that NCI-H1299 was less sensitive to platinum drugs than other lung cancer cell lines at a lower concentration, and this type of lung cancer would be difficult to treat with chemotherapy. Therefore, it is necessary to find a potential strategy for this type of lung cancer to improve the cure rate.

PET tracking of PD-L1 in vivo

To validate the specificity of ^{68}Ga-NOTA-Nb109 to endogenous PD-L1 in vivo, PET imaging was employed on the nude mice bearing tumor xenografts with different PD-L1 expression, and the representative PET images are displayed in Figs. 3, 4, 5 and 6. It is obvious that the PET imaging on U87 xenografts showed significantly higher accumulation of ^{68}Ga-NOTA-Nb109 at the tumor site and a good delineation of the tumor persisted until the end of imaging session (Fig. 3a). According to the ROI analysis of biodistribution quantification, the maximum uptake within U87 tumor was 2.84 ± 0.32%ID/g at 10 min

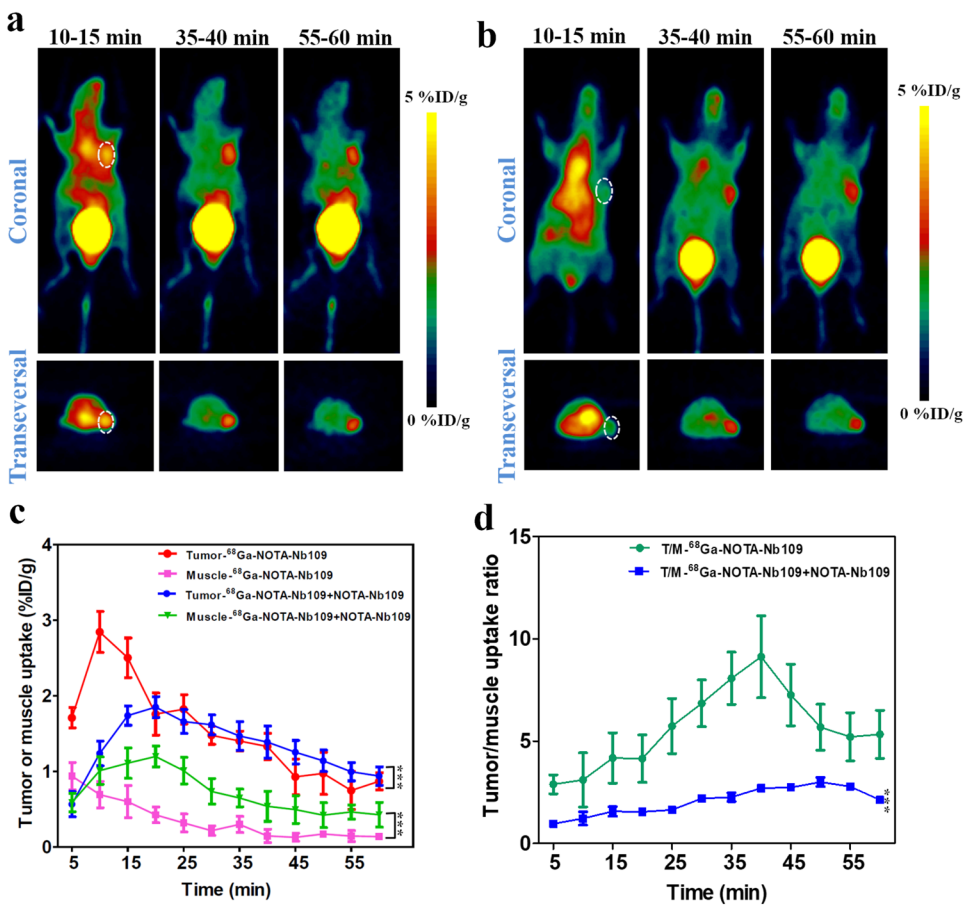

Fig. 3 MicroPET imaging of U87-bearing model with ^{68}Ga-NOTA-Nb109. **a** Representative PET images of U87 xenograft obtained at different time points after injection of ^{68}Ga-NOTA-Nb109. **b** Representative PET images of U87 xenograft pretreated with non-labeled probe for 30 min before injection of ^{68}Ga-NOTA-Nb109. The tumor was denoted with a dotted line circle. **c** Tissue uptake of ^{68}Ga-NOTA-Nb109 in U87 xenograft quantified by ROI analysis over the imaging time-course. **d** Tumor-to-muscle uptake ratio for ^{68}Ga-NOTA-Nb109 in U87 xenograft over time. All data were expressed as mean ± SD (n = 3). ***P < 0.001

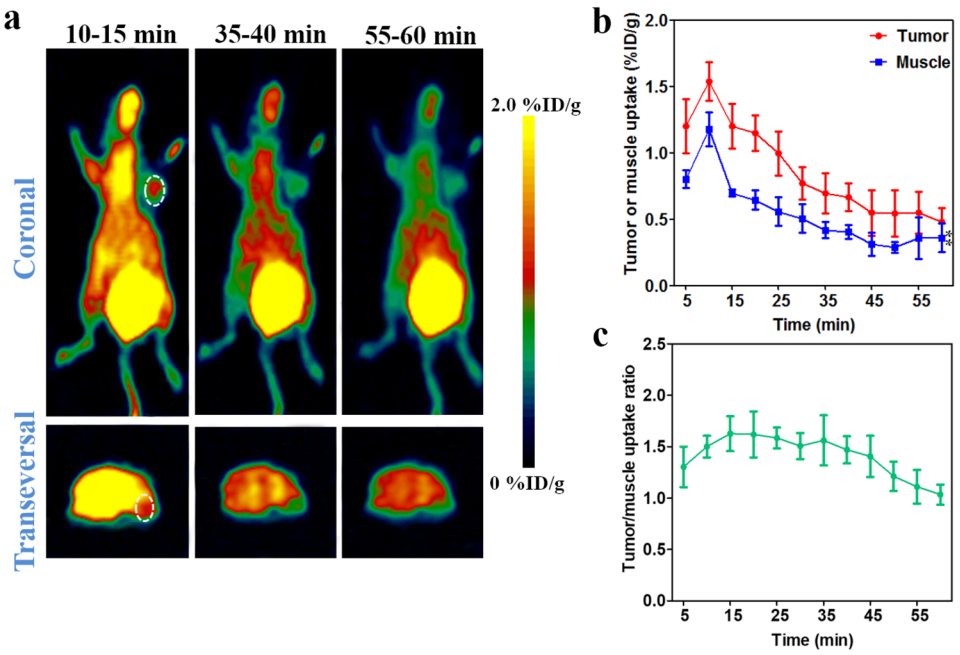

Fig. 4 MicroPET imaging of HCT 116-bearing model with ^{68}Ga-NOTA-Nb109. **a** Representative PET images of HCT 116 xenograft obtained at different time points after injection of ^{68}Ga-NOTA-Nb109. The tumor was denoted with a dotted line circle. **b** Tissue uptake of ^{68}Ga-NOTA-Nb109 in HCT 116 xenograft quantified by ROI analysis over the imaging time-course. **c** Tumor-to-muscle uptake ratio for ^{68}Ga-NOTA-Nb109 in HCT 116 xenograft over time. All data were expressed as mean ± SD ($n = 3$). $^{**}P < 0.01$

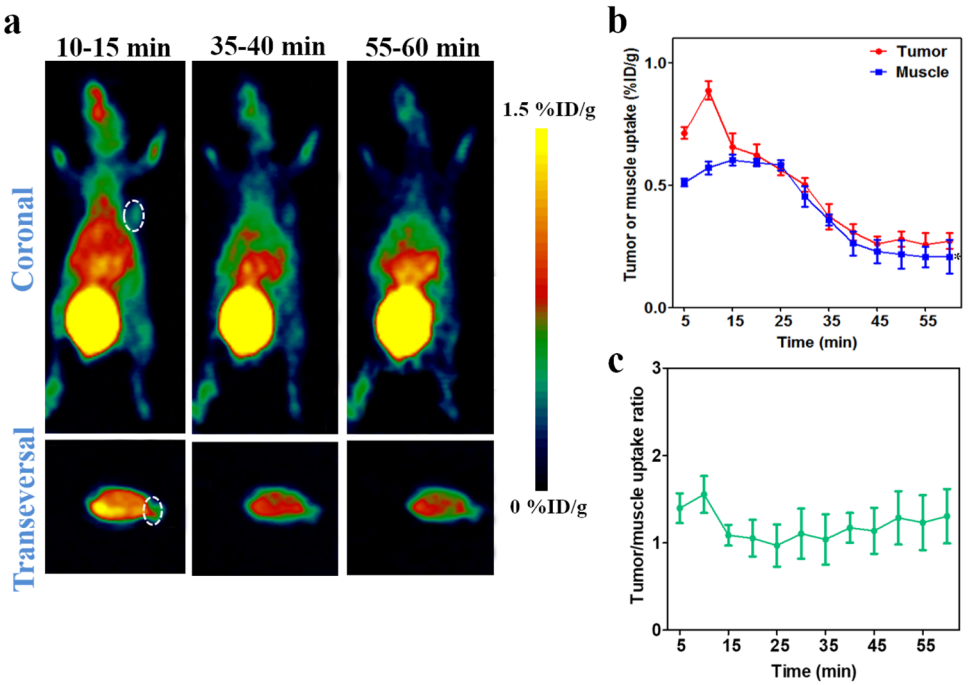

Fig. 5 MicroPET imaging of NCI-H1299-bearing model with ^{68}Ga-NOTA-Nb109. **a** Representative PET images of NCI-H1299 xenograft obtained at different time points after injection of ^{68}Ga-NOTA-Nb109. The tumor was denoted with a dotted line circle. **b** Tumor uptake of ^{68}Ga-NOTA-Nb109 in NCI-H1299 xenograft quantified by ROI analysis over the imaging time-course. **c** Tumor-to-muscle uptake ratio for ^{68}Ga-NOTA-Nb109 in NCI-H1299 xenograft over time. All data were expressed as mean ± SD ($n = 3$). $^{*}P < 0.05$

post-injection and it was significantly higher than that in muscle (Fig. 3c), indicating that the tracer can rapidly and specifically bind to the target. The heart uptake was significantly high at the first 15 min post-injection, but it was almost fully cleared at 35 min post-injection. The higher uptake of bladder throughout the whole PET imaging process indicated that the tracer was cleared mainly via the renal pathway. Although the absolute uptake of ^{68}Ga-NOTA-Nb109 in U87 tumor decreased over time, the tracer exhibited a favorable tumor-to-muscle ratio throughout the study, and the ratio can reach 9.12 ± 1.87 at 40 min post-injection (Fig. 3d).

In addition, the specificity of ^{68}Ga-NOTA-Nb109 to PD-L1 in vivo was further evidenced by the blocking assay in U87 tumors. The models were pretreated with 200-fold molar excess of non-labeled tracer (about 0.4 mg in 200 μL normal saline) for 30 min. PET imaging illustrated in Fig. 3b showed that the uptake of ^{68}Ga-NOTA-Nb109 in U87 tumors

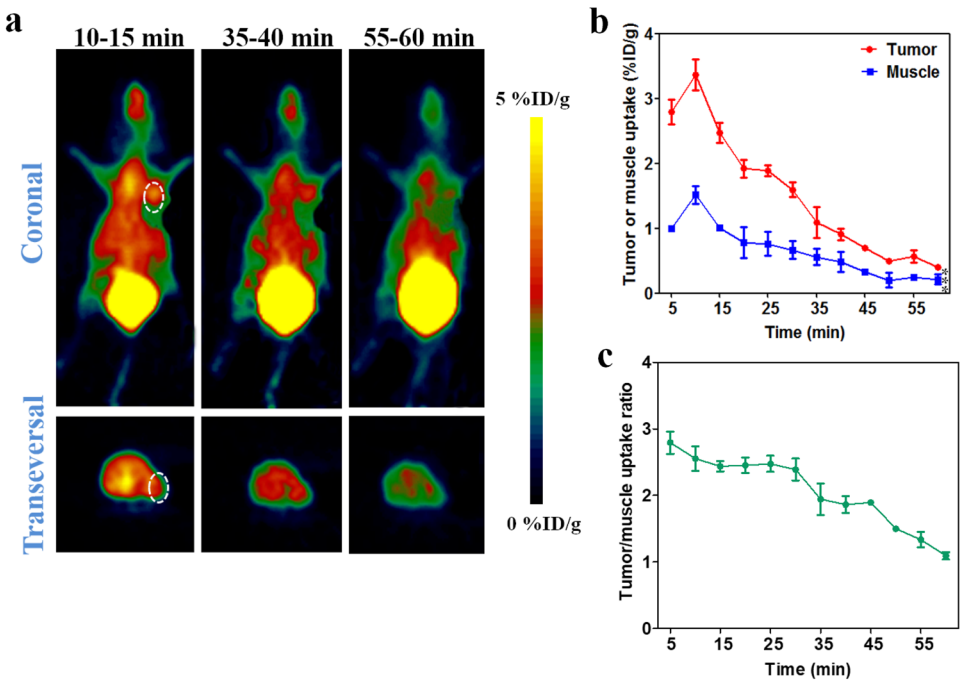

Fig. 6 MicroPET imaging of NCI-H1299-CDDP-bearing model with ^{68}Ga-NOTA-Nb109. **a** Representative PET images of NCI-H1299-CDDP xenograft obtained at different time points after injection of ^{68}Ga-NOTA-Nb109. The tumor was denoted with a dotted line circle. **b** Tissue uptake of ^{68}Ga-NOTA-Nb109 in NCI-H1299-CDDP xenograft quantified by ROI analysis over the imaging time-course. **c** Tumor-to-muscle uptake ratio for ^{68}Ga-NOTA-Nb109 in NCI-H1299-CDDP xenograft over time. All data were expressed as mean ± SD ($n = 3$). ***$P < 0.001$

was significantly blocked within the first 20 min post-injection. The maximum uptake was only 1.76 ± 0.14%ID/g at 20 min post-injection, and it was delayed by 10 min compared with non-blocking group. With the injection of non-labeled tracer, the clearance of tracer from the tumor and muscle became slow, and a clear tumor image can still be observed at 35 min post-injection (Fig. 3b), which might be attributed to the rapid clearance of non-labeled tracer from body. The tumor-to-muscle uptake ratio increased gradually and reached the highest peak (3.00 ± 0.22) at 50 min post-injection. The results suggested that the non-labeled tracer can block the uptake of ^{68}Ga-NOTA-Nb109 in tumors.

The specificity of ^{68}Ga-NOTA-Nb109 to PD-L1 was also evaluated in HCT 116 (Fig. 4) and NCI-H1299 (Fig. 5) xenografts with medium and low PD-L1 expression level, respectively. The PET images displayed a remarkably decreased tumor uptake of ^{68}Ga-NOTA-Nb109 in HCT 116 and NCI-H1299 compared to that in U87, and the accumulation of ^{68}Ga-NOTA-Nb109 in HCT 116 xenografts (Fig. 4a) was higher than that in NCI-H1299 (Fig. 5a). The ROI analysis showed that both HCT 116 and NCI-H1299 xenografts reached the maximum tumor uptake at 10 min post-injection, and the highest accumulation of radioactivity was 1.54 ± 0.14 and 0.88 ± 0.037%ID/g (Figs. 4b, and 5b), respectively. In addition, comparison of tumor-to-muscle uptake ratio between HCT 116 and NCI-H1299 xenografts also revealed that tracer ^{68}Ga-NOTA-Nb109 can accurately detect the different expression level of PD-L1 in various tumors (Fig. 4c and 5c). Overall, the in vivo PET imaging results were in good agreement with the in vitro flow cytometry and Western blot analysis of PD-L1 expression level, suggesting that tracer ^{68}Ga-NOTA-Nb109 can sensitively and specifically monitor the PD-L1 expression.

Given that more epitopes of PD-L1 can be induced by chemotherapy, the change of PD-L1 expression in NCI-H1299 tumor xenografts treated with CDDP was assessed using ^{68}Ga-NOTA-Nb109 (Fig. 6). There was no significant change in the volume of NCI-H1299 tumor after treatment of 2 mg/kg CDDP for three times, whereas the weight of the mice decreased slightly, suggesting that CDDP inhibited the development of tumor. As demonstrated by PET images in Fig. 6a, the tumor uptake of ^{68}Ga-NOTA-Nb109 increased remarkably after the treatment with CDDP, and reached the peak at 10 min post-injection. According to the ROI analysis of images, the accumulation of tracer in tumor of NCI-H1299-CDDP was 3.36 ± 0.23%ID/g at 10 min post-injection and it was 3.8-fold of that in NCI-H1299 (Fig. 6b). Meantime, the tumor-to-muscle uptake ratio after the treatment of CDDP was larger than that of the tumor without CDDP treatment, although the ratio decreased over time (Fig. 6c). PET studies revealed that the PD-L1 expression level was obviously induced by CDDP, and the upregulation of PD-L1 can be sensitively monitored by PET imaging with ^{68}Ga-NOTA-Nb109.

The specificity and sensitivity of tracer ^{68}Ga-NOTA-Nb109 to PD-L1 in NCI-H1299 and NCI-H1299-CDDP tumors were also evaluated by autoradiography. It was found from Fig. 7a that the grayscale in NCI-H1299-CDDP tumors was higher than that in NCI-H1299 tumors, indicating a higher accumulation of ^{68}Ga-NOTA-Nb109 was achieved in NCI-H1299-CDDP tumor and CDDP can upregulate the

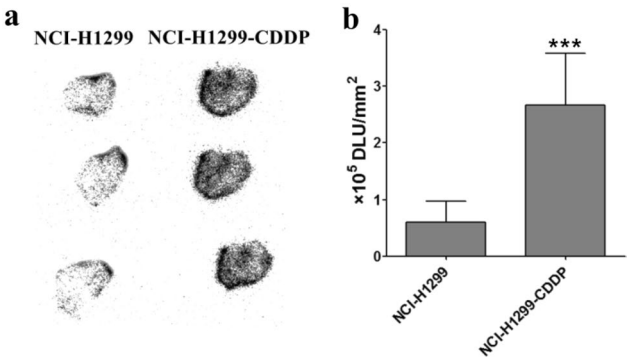

Fig. 7 Ex vivo distribution of ^{68}Ga-NOTA-Nb109 in tumor. **a** Autoradiography analysis of ^{68}Ga-NOTA-Nb109 in NCI-H1299 and CDDP-treated NCI-H1299 tumors at 60 min post injection. **b** Quantitative analysis of the accumulation of ^{68}Ga-NOTA-Nb109 in tumors by ImageJ software. $^{***}P < 0.001$

expression of PD-L1 in tumors. According to the grayscale analysis by ImageJ (Fig. 7b), the expression level of PD-L1 increased threefold by the treatment of CDDP, which was consistent with that determined by PET imaging.

^{18}F-FDG PET imaging

^{18}F-FDG is considered as a standard modality for staging and follow-up monitoring of cancers, and widely used in many immunotherapy setting [34–36]. In order to compare the effectiveness of ^{18}F-FDG and ^{68}Ga-NOTA-Nb109 in guiding immunotherapy, ^{18}F-FDG PET imaging of U87 and NCI-H1299-bearing models with different expression level of PD-L1 was performed. As illustrated in Fig. 8, the tracer ^{18}F-FDG accumulated quickly in U87 tumor and remained at a higher level with the tumor uptake of 13.59 ± 0.66%ID/g at 25 min post-injection, and the tumor uptake of ^{18}F-FDG in NCI-H1299 xenograft reached the maximum of 6.50 ± 0.12%ID/g at 10 min post-injection. However, it was noticed that internal organs with high-glucose metabolism such as heart, liver, and intestine, showed higher ^{18}F-FDG uptake than tumors over the imaging time course in both U87 and NCI-H1299 xenografts (Fig. 8a and b). The absorption of ^{18}F-FDG in internal organs with high-glucose metabolism resulted in unsatisfactory background uptake, and the maximum tumor-to-muscle uptake ratio was 4.25 ± 0.29 and 3.01 ± 0.18 in U87 and NCI-H1299 xenografts, respectively (Fig. 8d). In contrast with the tracer ^{68}Ga-NOTA-Nb109, although the tumor uptake of ^{18}F-FDG increased by about several folds, the accumulation of ^{18}F-FDG in internal

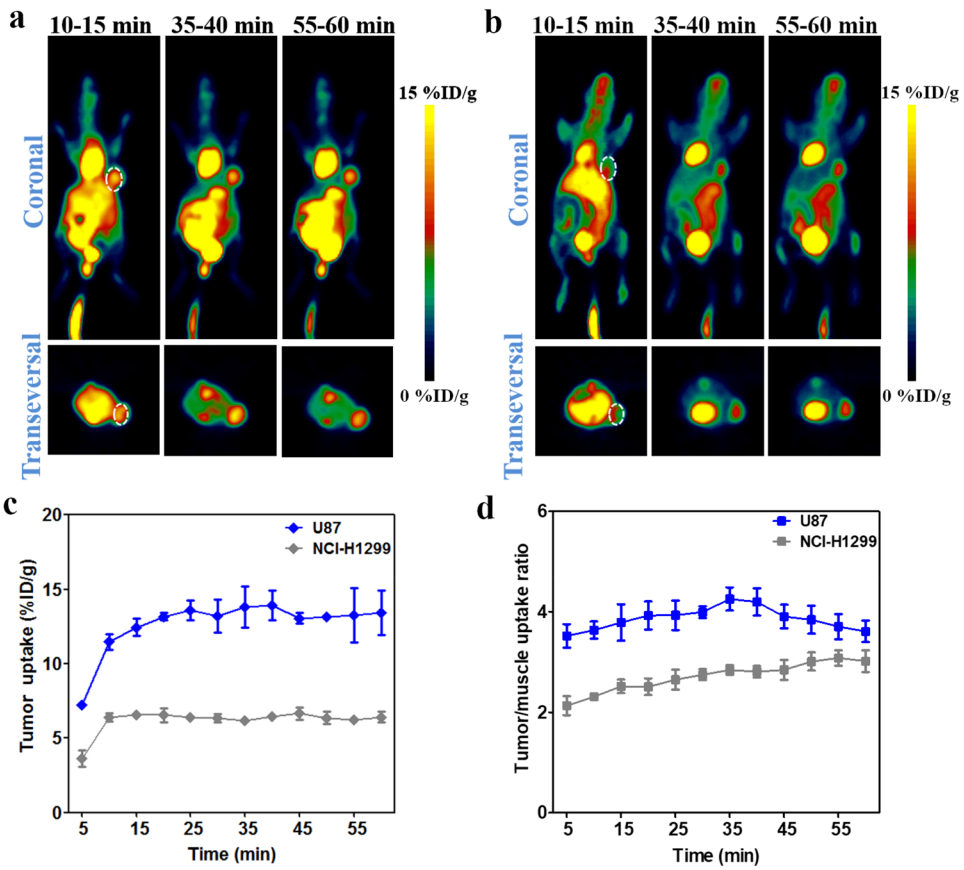

Fig. 8 MicroPET imaging of tumor-bearing models with ^{18}F-FDG. **a** Representative PET images of U87 xenograft obtained at different time points after injection of ^{18}F-FDG. **b** Representative PET images of NCI-H1299 xenograft obtained at different time points after injection of ^{18}F-FDG. The tumor was denoted with a dotted line circle. **c** Tumor uptake of ^{18}F-FDG in U87 and NCI-H1299 xenografts quantified by region of interest (ROI) analysis over the imaging time-course. **d** Tumor-to-muscle uptake ratio for ^{18}F-FDG in U87 and NCI-H1299 xenografts over time. All data were expressed as mean ± SD ($n = 3$)

organs was also very high. To better distinguish between the tumor and normal tissues, a high signal-to-noise ratio was necessary for the imaging tracer. Taken together, the tracer ^{68}Ga-NOTA-Nb109 with a higher tumor uptake and a lower background uptake could be a better choice to detect the PD-L1 expression in vivo.

Discussion

Immunotherapy is currently acknowledged as the most compelling strategy for cancers [37], and the immune checkpoint PD-1/PD-L1-based immunotherapy has become a vital part of the clinical treatment for cancers [38, 39]. To achieve desired curative effect, screening of cancers with high PD-L1 expression would be a primary challenge. Compared with IHC, PET imaging is widely used in the diagnosis of diseases owing to its high sensitivity, specificity, real-time imaging and non-invasiveness. Nowadays, a lot of PET tracers targeting PD-L1 have been developed, but these tracers are mainly radionuclide-labeled mAbs, such as ^{89}Zr-Atezolizumab and ^{64}Cu-Atezolizumab [18, 19, 23]. Although these probes can specifically target PD-L1 in vivo, it should take several days to obtain satisfactory visualization of tumor lesions. And the imaging efficiency of radionuclide-labeled mAbs in evaluating the PD-L1 expression or therapeutic effect would be affected by the treatment of therapeutic antibody since they targeted the same binding site. Moreover, the long-term metabolism of mAb-based probes might result in some immune-related adverse events [40]. Therefore, it is necessary to develop novel non-blocking tracers to monitor the PD-L1 expression, which should possess different binding sites from the available therapeutic agents. A non-blocking nanobody Nb109 has been explored in our previous work, and the specificity of ^{68}Ga-NOTA-Nb109 to PD-L1 was studied in A375-hPD-L1 tumor-bearing mice [20].

In this study, the potency of ^{68}Ga-NOTA-Nb109 in real-time detecting and quantifying the PD-L1 expression in different types of cancers was evaluated. It was more worth studying the binding specificity of a tracer to wild-type cancers than studying that to a genetically modified model. Therefore, the PD-L1 expression level in U87, HCT 116, and NCI-H1299 cancers was first evaluated by flow cytometry and Western blot methods, and the results demonstrated that the PD-L1 expression level was high in U87 cancer cells, followed by HCT 116 and NCI-H1299. In vitro cellular uptake illustrated that ^{68}Ga-NOTA-Nb109 can be used to sensitively and specifically detect the varying PD-L1 expression level in cancer cells.

PET imaging of U87, HCT 116, and NCI-H1299 xenografts showed that tracer ^{68}Ga-NOTA-Nb109 can specifically bind to PD-L1, and the tumor uptake corresponded with the PD-L1 expression level. The PET signal in the body decreased rapidly with the clearance of tracer, resulting in a good tumor uptake, especially for U87 tumor-bearing mice with high PD-L1 expression. The blocking assay further evidenced that ^{68}Ga-NOTA-Nb109 can specifically bind to PD-L1 in tumors. PET imaging of different tumor-bearing models using our tracer ^{68}Ga-NOTA-Nb109 showed high-tumor uptake at 10 min post-injection, whereas a satisfactory visualization of tumor could be obtained at 1–2 days and 4–7 days post-injection for mAb-based probes ^{64}Cu-Atezolizumab and ^{89}Zr-Atezolizumab, respectively [18, 19, 23]. Comparison of these probes indicated that the probe ^{68}Ga-NOTA-Nb109 was more suitable for clinical applications owing to its specific targeting and rapid clearance from body. Although the accumulation and tumor-to-muscle uptake ratio of ^{68}Ga-NOTA-Nb109 in U87 xenograft were slightly lower than those in A375-hPD-L1 [20], the encouraging results are of great importance to guide the immunotherapy and efficacy evaluation.

Lung cancer has become a major disease that threatens human health due to its poor prognosis and lacking of targeted drugs. Combination of surgical and chemotherapy is the most common treatment strategy for lung cancers, in which platinum is the first-line clinical chemotherapy drug [32, 41]. Although the 5-year survival rate of patients was increased using multiple therapeutic modalities, the acquired resistance to platinum-based drugs still limited their widespread clinical applications. Studies showed that PD-L1 was highly expressed in most lung cancers, and immunotherapy targeted blocking the pathway of PD-1/PD-L1 could be effective in raising life quality and prolonging life survival of patients. However, some lung cancers with low PD-L1 expression such as NCI-H1299 showed little response or resistance to the immunotherapy. Therefore, we need to upregulate the expression of PD-L1 in these lung cancers, which might be beneficial for improving the efficacy of immunotherapy. It has been reported that chemotherapy drugs such as CDDP can upregulate the expression of PD-L1 in most cancers [31–33]. Therefore, in the present study, the expression of PD-L1 in NCI-H1299 cells regulated by CDDP was studied and the results showed that the PD-L1 expression level was improved by threefold at 20 μM CDDP. Cytotoxicity assay also demonstrated that lung cancer cell line NCI-H1299 was more resistant to the chemotherapy of CDDP than other lung cancer cell lines. Therefore, a combination of immunotherapy and chemotherapy could be employed as a better strategy to improve therapeutic effect of this type lung cancer.

To evaluate the sensitivity and specificity of ^{68}Ga-NOTA-Nb109 in monitoring the change of PD-L1 expression, in vitro cellular uptake and in vivo PET imaging were studied. The cellular uptake of tracer ^{68}Ga-NOTA-Nb109 in NCI-H1299 with treatment of CDDP was about twofold of that in NCI-H1299 without treatment of CDDP. PET

imaging showed a satisfactory visualization of tumor lesions in NCI-H1299-CDDP-bearing models, and the tumor accumulation of ^{68}Ga-NOTA-Nb109 was improved 3.8-fold in comparison with that in NCI-H1299-bearing models without treatment of CDDP. Compared with the PET imaging results of U87 tumor-bearing models, the signal-to-noise ratio was unsatisfactory although the accumulation of radioactivity in NCI-H1299-CDDP tumors was higher. This might be attributed to the systemic toxicity of CDDP, which upregulated the expression of PD-L1 in other tissues. Furthermore, the specificity of ^{68}Ga-NOTA-Nb109 to PD-L1 was verified by autoradiography analysis. The results demonstrated that in vivo expression of PD-L1 can be upregulated by the treatment of CDDP, and the change of PD-L1 expression in tumors can be sensitively detected by the tracer ^{68}Ga-NOTA-Nb109.

^{18}F-FDG is a widely-used radiotracer for tumor imaging and used to guide the immunotherapy and evaluate therapeutic efficacy [36, 42]. In the present study, we also carried out PET imaging of ^{18}F-FDG in U87 and NCI-H1299 xenografts with different PD-L1 expression level. Both U87 and NCI-H1299 tumors showed high uptake of ^{18}F-FDG, although the PD-L1 expression level was different in these two cancer cells. This suggested that ^{18}F-FDG lacks specificity to PD-L1 in tumors although it can be used for tumor imaging. In contrast, ^{68}Ga-NOTA-Nb109 showed significantly different accumulations in PD-L1 positive and negative tumors, implying that it was more specific than ^{18}F-FDG. In addition, the tracer ^{68}Ga-NOTA-Nb109 showed lower background uptake and a higher signal-to-noise ratio than ^{18}F-FDG in U87 xenografts, further suggesting that ^{68}Ga-NOTA-Nb109 was a specific PD-L1-targeting tracer. It not only can help screen patients with high PD-L1 expression, but also can guide the immunotherapy of cancers by targeting PD-L1.

In conclusion, specificity and sensitivity of a non-blocking PET imaging tracer ^{68}Ga-NOTA-Nb109 in monitoring the PD-L1 expression were evaluated. In vitro cell uptake studies and in vivo PET imaging studies correlated well with the PD-L1 expression level detected in vitro, and the change of PD-L1 expression induced by chemotherapy can be sensitively detected by ^{68}Ga-NOTA-Nb109 in vitro and in vivo. PET imaging of ^{68}Ga-NOTA-Nb109 and ^{18}F-FDG in tumor-bearing models with different expression level of PD-L1 indicated ^{68}Ga-NOTA-Nb109 was more promising to accurately detect PD-L1 expression in vivo. The encouraging results suggest that ^{68}Ga-NOTA-Nb109 can be used for real-time, sensitively, and specifically monitoring the change of PD-L1 expression in cancers, which will provide instructive information for the selection of personalized treatment options and the evaluation of prognostic efficacy.

Acknowledgements The nanobody of NOTA-Nb109 was kindly provided by Suzhou Smart Nuclide Biopharmaceutical Co., Ltd, China.

Authors' contributions QL and LJ performed the experiments, acquired and analyzed the data. QL wrote the paper, and LJ contributed to paper writing. KL and GL contributed to the PET imaging, and analyzed data for in vivo experiments. HL performed the probe labeling and quality control. JL and LQ conceived, designed, and supported the study, interpreted the results and revised the manuscript.

Funding This work was funded by the National Natural Science Foundation of China (81972906, 81971645, and 22076069), Natural Science Foundation of Jiangsu Province (BK20181128 and BK20201135), Key Youth Medical Talent Project of Jiangsu Province (QNRC2016626 and QNRC2016629), Jiangsu Commission of Health (ZDA2020007 and M2020028), Precision Medical Project of Wuxi Commission of Health and Family Planning (J201806), Major Scientific Research Project of Wuxi Commission of Health (Z201913), and Innovation Capacity Development Plan of Jiangsu Province (BM2018023).

Compliance with ethical standards

Conflict of interest The authors declare that they have no conflict of interest.

Ethical approval All applicable international, national, and/or institutional guidelines for the care and use of animals were followed. All animal procedures were performed according to the protocols approved by the ethical committee of Jiangsu Institute of Nuclear Medicine.

References

1. Dal Bello MG, Alama A, Coco S, Vanni I, Grossi F (2017) Understanding the checkpoint blockade in lung cancer immunotherapy. Drug Discov Today. 22(8):1266–1273. https://doi.org/10.1016/j.drudis.2017.05.016
2. Pardoll DM (2012) The blockade of immune checkpoints in cancer immunotherapy. Nat Rev Cancer 12(4):252–264. https://doi.org/10.1038/nrc3239
3. Hira R, Francisco S-V, Konnor L, Walid C, Philip J, Darragh H et al (2018) Molecular determinants of response to anti-programmed cell death (PD)-1 and anti-programmed death-ligand 1 (PD-L1) blockade in patients with non-small-cell lung cancer profiled with targeted next-generation sequencing. J Clin Oncol 36(7):633–641. https://doi.org/10.1200/JCO.2017.75.3384
4. Ferrara R, Mezquita L, Texier M, Lahmar J, Audigier-Valette C, Tessonnier L et al (2018) Hyperprogressive disease in patients with advanced non-small cell lung cancer treated with PD-1/PD-L1 inhibitors or with single-agent chemotherapy. JAMA Oncol. 4(11):1543–1552. https://doi.org/10.1001/jamaoncol.2018.3676
5. Bellmunt J, Powles T, Vogelzang NJ (2017) A review on the evolution of PD-1/PD-L1 immunotherapy for bladder cancer: the future is now. Cancer Treat Rev 54:58–67. https://doi.org/10.1016/j.ctrv.2017.01.007
6. Jung HI, Jeong D, Ji S, Ahn TS, Bae SH, Chin S et al (2017) Overexpression of PD-L1 and PD-L2 is associated with poor prognosis in patients with hepatocellular carcinoma. Cancer Res Treat. 49(1):246–254. https://doi.org/10.4143/crt.2016.066
7. Rezaeeyan H, Hassani SN, Barati M, Shahjahani M, Saki N (2017) PD-1/PD-L1 as a prognostic factor in leukemia. J Hematopathol. 10(1):17–24. https://doi.org/10.1007/s12308-017-0293-z
8. Postow MA, Callahan MK, Wolchok JD (2015) Immune Checkpoint Blockade in Cancer Therapy. J Clin Oncol 33(17):1974–1982. https://doi.org/10.1200/JCO.2014.59.4358

9. Cheng M, Durm G, Hanna N, Einhorn LH, Kong FS (2017) Can radiotherapy potentiate the effectiveness of immune checkpoint inhibitors in lung cancer? Future Oncol. 13(28):2503–2505. https://doi.org/10.2217/fon-2017-0405
10. Ohaegbulam KC, Assal A, Lazar-Molnar E, Yao Y, Zang X (2015) Human cancer immunotherapy with antibodies to the PD-1 and PD-L1 pathway. Trends Mol Med. 21(1):24–33. https://doi.org/10.1016/j.molmed.2014.10.009
11. Gibney GT, Weiner LM, Atkins MB (2016) Predictive biomarkers for checkpoint inhibitor-based immunotherapy. Lancet Oncol 17(12):e542–e551. https://doi.org/10.1016/s1470-2045(16)30406-5
12. Wang X, Teng F, Kong L, Yu J (2016) PD-L1 expression in human cancers and its association with clinical outcomes. Onco Targets Ther. 9:5023–5039. https://doi.org/10.2147/OTT.S105862
13. Aguiar PN, Andrade DMR, Peter H, Hakaru T, Gilberto DL (2017) PD-L1 expression as a predictive biomarker in advanced non-small-cell lung cancer: updated survival data. Immunotherapy. 9(6):499–506
14. Topalian SL, Taube JM, Anders RA, Pardoll DM (2016) Mechanism-driven biomarkers to guide immune checkpoint blockade in cancer therapy. Nat Rev Cancer 16(5):275–287. https://doi.org/10.1038/nrc.2016.36
15. Rehman JA, Han G, Carvajal-Hausdorf DE, Wasserman BE, Pelekanou V, Mani NL et al (2017) Quantitative and pathologist-read comparison of the heterogeneity of programmed death-ligand 1 (PD-L1) expression in non-small cell lung cancer. Mod Pathol 30(3):340–349. https://doi.org/10.1038/modpathol.2016.186
16. Hirsch FR, McElhinny A, Stanforth D, Ranger-Moore J, Jansson M, Kulangara K et al (2017) PD-L1 immunohistochemistry assays for lung cancer: results from phase 1 of the blueprint PD-L1 IHC assay comparison project. J Thorac Oncol. 12(2):208–222. https://doi.org/10.1016/j.jtho.2016.11.2228
17. Patel SP, Kurzrock R (2015) PD-L1 Expression as a Predictive Biomarker in Cancer Immunotherapy. Mol Cancer Ther 14(4):847–856. https://doi.org/10.1158/1535-7163.MCT-14-0983
18. Lesniak WG, Chatterjee S, Gabrielson M, Lisok A, Wharram B, Pomper MG et al (2016) PD-L1 detection in tumors using [(64)Cu]Atezolizumab with PET. Bioconjug Chem 27(9):2103–2110. https://doi.org/10.1021/acs.bioconjchem.6b00348
19. Bensch F, van der Veen EL, Lub-de Hooge MN, Jorritsma-Smit A, Boellaard R, Kok IC et al (2018) (89)Zr-atezolizumab imaging as a non-invasive approach to assess clinical response to PD-L1 blockade in cancer. Nat Med 24(12):1852–1858. https://doi.org/10.1038/s41591-018-0255-8
20. Lv G, Sun X, Qiu L, Sun Y, Li K, Liu Q et al (2020) PET imaging of tumor PD-L1 expression with a highly specific nonblocking single-domain antibody. J Nucl Med 61(1):117–122. https://doi.org/10.2967/jnumed.119.226712
21. Inman BA, Longo TA, Ramalingam S, Harrison MR (2017) Atezolizumab: a PD-L1-blocking antibody for bladder cancer. Clin Cancer Res 23(8):1886–1890. https://doi.org/10.1158/1078-0432.CCR-16-1417
22. Seetharamu N, Preeshagul IR, Sullivan KM (2017) New PD-L1 inhibitors in non-small cell lung cancer-impact of atezolizumab. Lung Cancer 8:67–78. https://doi.org/10.2147/LCTT.S113177
23. Vento J, Mulgaonkar A, Woolford L, Nham K, Christie A, Bagrodia A et al (2019) PD-L1 detection using (89)Zr-atezolizumab immuno-PET in renal cell carcinoma tumorgrafts from a patient with favorable nivolumab response. J Immunother Cancer. 7(1):144. https://doi.org/10.1186/s40425-019-0607-z
24. De Silva RA, Kumar D, Lisok A, Chatterjee S, Wharram B, Venkateswara Rao K et al (2018) Peptide-based (68)Ga-PET radiotracer for imaging PD-L1 expression in cancer. Mol Pharm 15(9):3946–3952. https://doi.org/10.1021/acs.molpharmaceut.8b00399
25. Kumar D, Lisok A, Dahmane E, McCoy M, Shelake S, Chatterjee S et al (2019) Peptide-based PET quantifies target engagement of PD-L1 therapeutics. J Clin Invest. 129(2):616–630. https://doi.org/10.1172/JCI122216
26. Hu K, Kuan H, Hanyu M, Masayuki H, Xie L, Zhang Y et al (2019) Developing native peptide-based radiotracers for PD-L1 PET imaging and improving imaging contrast by pegylation. Chem Commun 55(29):4162–4165. https://doi.org/10.1039/c9cc00445a
27. Pilotto S, Molina-Vila MA, Karachaliou N, Carbognin L, Viteri S, Gonzalez-Cao M et al (2015) Integrating the molecular background of targeted therapy and immunotherapy in lung cancer: a way to explore the impact of mutational landscape on tumor immunogenicity. Transl Lung Cancer Res. 4(6):721–727. https://doi.org/10.3978/j.issn.2218-6751.2015.10.11
28. Ehlerding EB, Lee HJ, Barnhart TE, Jiang D, Kang L, McNeel DG et al (2019) Noninvasive imaging and quantification of radiotherapy-induced PD-L1 upregulation with (89)Zr-Df-Atezolizumab. Bioconjug Chem 30(5):1434–1441. https://doi.org/10.1021/acs.bioconjchem.9b00178
29. Mok TSK, Wu Y-L, Kudaba I, Kowalski DM, Cho BC, Turna HZ et al (2019) Pembrolizumab versus chemotherapy for previously untreated, PD-L1-expressing, locally advanced or metastatic non-small-cell lung cancer (KEYNOTE-042): a randomised, open-label, controlled, phase 3 trial. Lancet. 393(10183):1819–1830. https://doi.org/10.1016/s0140-6736(18)32409-7
30. Reck M, Rodriguez-Abreu D, Robinson AG, Hui R, Csoszi T, Fulop A et al (2019) Updated analysis of KEYNOTE-024: pembrolizumab versus platinum-based chemotherapy for advanced non-small-cell lung cancer with PD-L1 tumor proportion score of 50% or greater. J Clin Oncol 37(7):537–546
31. Yan F, Pang J, Peng Y, Molina JR, Yang P, Liu S (2016) Elevated cellular PD1/PD-L1 expression confers acquired resistance to cisplatin in small cell lung cancer cells. PLoS ONE 11(9):e0162925. https://doi.org/10.1371/journal.pone.0162925
32. Wangpaichitr M, Kandemir H, Li YY, Wu C, Nguyen D, Feun LG et al (2017) Relationship of Metabolic Alterations and PD-L1 Expression in Cisplatin Resistant Lung Cancer. Cell Dev Biol. 6(2):183. https://doi.org/10.4172/2168-9296.1000183
33. Fournel L, Wu Z, Stadler N, Damotte D, Lococo F, Boulle G et al (2019) Cisplatin increases PD-L1 expression and optimizes immune check-point blockade in non-small cell lung cancer. Cancer Lett 464:5–14. https://doi.org/10.1016/j.canlet.2019.08.005
34. Chen R, Zhou X, Liu J, Huang G (2019) Relationship between the expression of PD-1/PD-L1 and (18)F-FDG uptake in bladder cancer. Eur J Nucl Med Mol Imaging. 46(4):848–854. https://doi.org/10.1007/s00259-018-4208-8
35. Jreige M, Letovanec I, Chaba K, Renaud S, Rusakiewicz S, Cristina V et al (2019) (18)F-FDG PET metabolic-to-morphological volume ratio predicts PD-L1 tumour expression and response to PD-1 blockade in non-small-cell lung cancer. Eur J Nucl Med Mol Imaging. 46(9):1859–1868. https://doi.org/10.1007/s00259-019-04348-x
36. Ehlerding EB, Lan X, Cai W (2019) Predicting PD-1/PD-L1 status in bladder cancer with (18)F-FDG PET? Eur J Nucl Med Mol Imaging. 46(4):791–793. https://doi.org/10.1007/s00259-018-4224-8
37. Wang X, Huang S, Zhang Y, Zhu L, Wu X (2018) The application and mechanism of PD pathway blockade for cancer therapy. Postgrad Med J 94(1107):53–60. https://doi.org/10.1136/postgradmedj-2017-135187
38. Chen L, Han X (2015) Anti-PD-1/PD-L1 therapy of human cancer: past, present, and future. J Clin Invest. 125(9):3384–3391. https://doi.org/10.1172/JCI80011
39. Constantinidou A, Alifieris C, Trafalis DT (2019) Targeting programmed cell death -1 (PD-1) and ligand (PD-L1): a new era in

cancer active immunotherapy. Pharmacol Ther 194:84–106. https://doi.org/10.1016/j.pharmthera.2018.09.008

40. Wang PF, Chen Y, Song SY, Wang TJ, Ji WJ, Li SW et al (2017) Immune-Related Adverse Events Associated with Anti-PD-1/PD-L1 Treatment for Malignancies: a Meta-Analysis. Front Pharmacol. 8:730. https://doi.org/10.3389/fphar.2017.00730
41. Guo D, Li M, Chen D, Jing W, Zhu H, Fu L et al (2019) Neutrophil-to-lymphocyte ratio is superior to platelet-to-lymphocyte ratio as a prognostic predictor in advanced non-small-cell lung cancer treated with first-line platinum-based chemotherapy. Future Oncol. 15(6):625–635
42. Takada K, Toyokawa G, Okamoto T, Baba S, Kozuma Y, Matsubara T et al (2017) Metabolic characteristics of programmed cell death-ligand 1-expressing lung cancer on (18) F-fluorodeoxyglucose positron emission tomography/computed tomography. Cancer Med 6(11):2552–2561. https://doi.org/10.1002/cam4.1215